Table S 1: Mean sensible heat flux (W m^{-2}) in arctic basins as parameterized in ERA5 in 1980–2000 (I) and 2001–2021 (II).

Season	**NDJ**		**FMA**		**MJJ**		**ASO**	
Time period	I	II	I	II	I	II	I	II
Central Arctic	0	2	-1	2	-1	0	0	1
Beaufort Sea	1	1	0	1	0	1	-1	-2
Chukchi Sea	-4	-8	0	0	1	1	-5	-7
East Siberian Sea	2	1	1	1	1	1	0	-2
Laptev Sea	0	0	0	0	1	1	-1	-2
Kara Sea	-2	-7	0	-2	1	0	-2	-3
Barents Sea	-34	-33	-23	-29	-2	-2	-10	-8
Greenland Sea	-31	-28	-26	-27	-3	-3	-9	-8
Baffin Bay	-13	-15	-9	-11	0	0	-3	-3

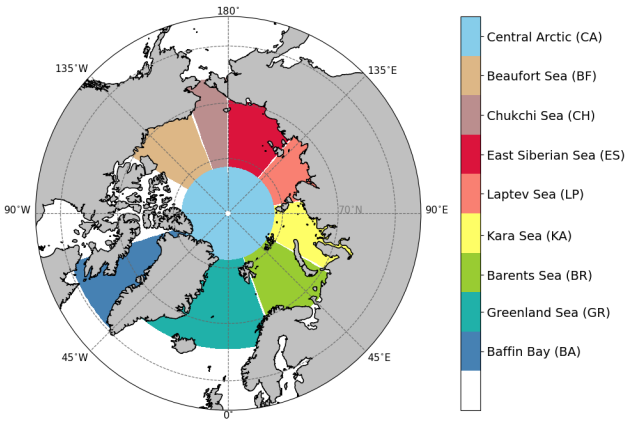

Figure S 1: Arctic basins used for calculating daily field means of sensible heat flux in Table S1 and Figure S2.

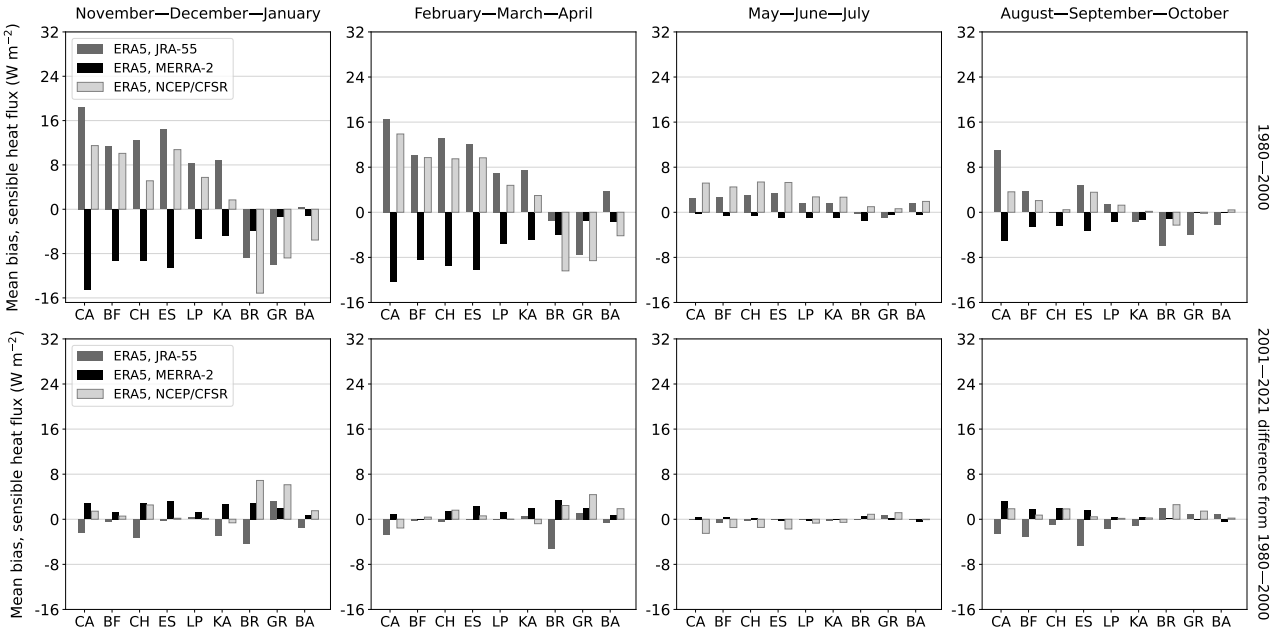

Figure S 2: Mean biases of daily field means of sensible heat flux between ERA5 and JRA-55 (grey), ERA5 and MERRA-2 (black), and ERA5 and NCEP/CFSR (light grey). Horizontal axis refers to arctic basins as seen in Figure S1. The first row shows data from period 1980–2000 and the second row the 2001–2021 difference from the earlier period. Only grid cells fully covered by the sea were considered in this analysis.

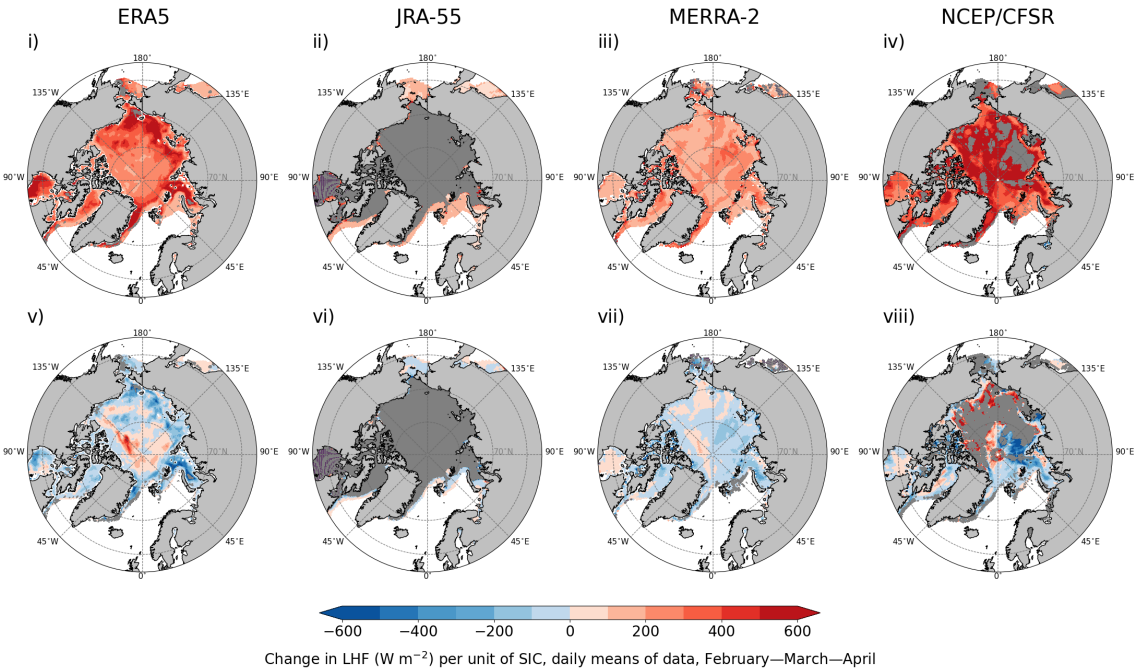

Figure S 3: Change in latent heat flux (W m^{-2}) per unit of change in sea-ice concentration (slope of regression line) in four reanalyses (columns), marine Arctic, FMA, based on the linear orthogonal-distance-regression (ODR) model. **i–iv** depict the period 1980–2000, **v–viii** show the 2001–2021 difference from 1980–2000. Dark grey indicates areas where the ODR model did not converge; in v–viii, dark grey shows these areas in 1980–2000 and/or 2001–2021. Only grid cells with a mean of SIC > 0.5 were considered, and only statistically significant results within 95 % confidence interval are shown.

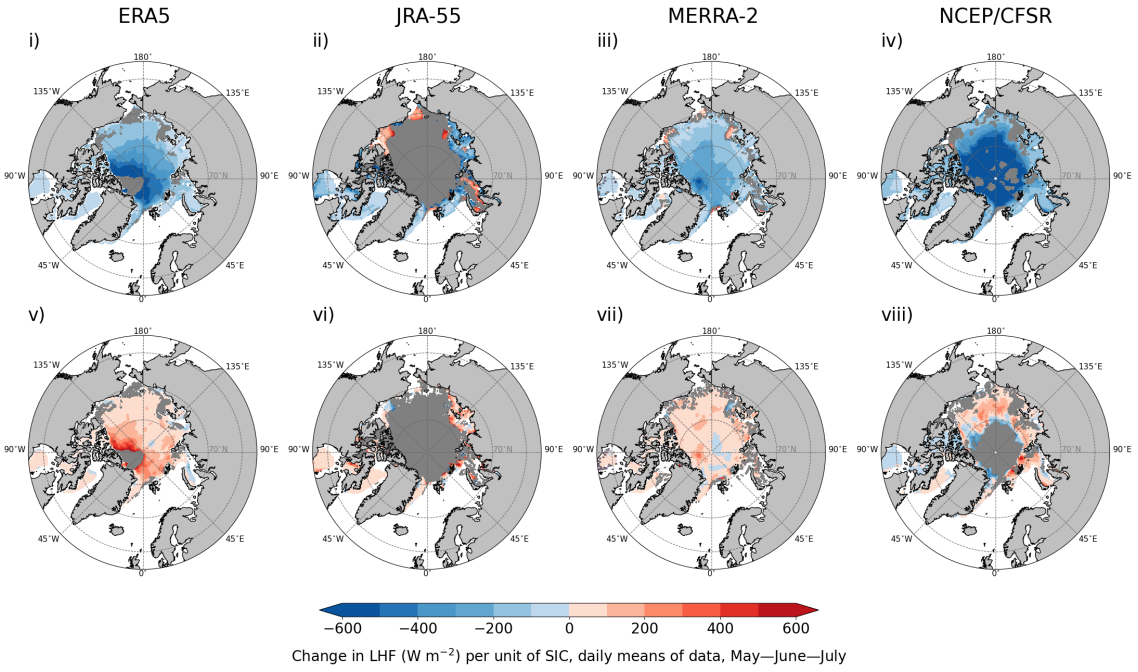

Figure S 4: Change in latent heat flux (W m^{-2}) per unit of change in sea-ice concentration (slope of regression line) in four reanalyses (columns), marine Arctic, MJJ, based on the linear orthogonal-distance-regression (ODR) model. **i–iv** depict the period 1980–2000, **v–viii** show the 2001–2021 difference from 1980–2000. Dark grey indicates areas where the ODR model did not converge; in v–viii, dark grey shows these areas in 1980–2000 and/or 2001–2021. Only grid cells with a mean of SIC > 0.5 were considered, and only statistically significant results within 95 % confidence interval are shown.

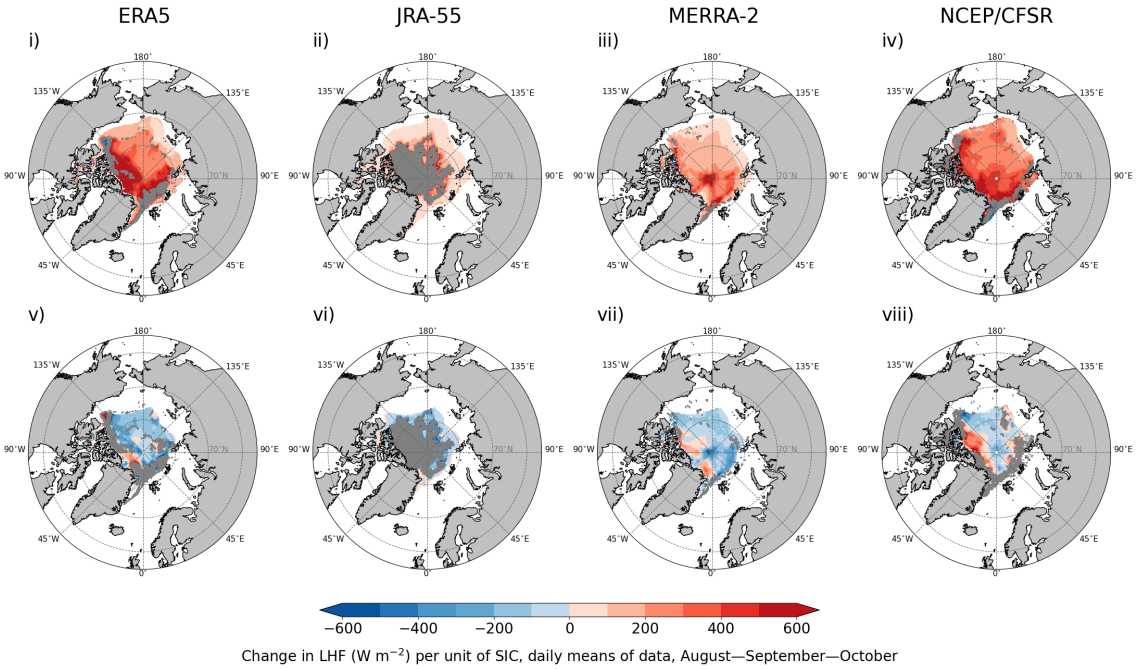

Figure S 5: Change in latent heat flux (W m^{-2}) per unit of change in sea-ice concentration (slope of regression line) in four reanalyses (columns), marine Arctic, ASO, based on the linear orthogonal-distance-regression (ODR) model. **i–iv** depict the period 1980–2000, **v–viii** show the 2001–2021 difference from 1980–2000. Dark grey indicates areas where the ODR model did not converge; in v–viii, dark grey shows these areas in 1980–2000 and/or 2001–2021. Only grid cells with a mean of SIC > 0.5 were considered, and only statistically significant results within 95 % confidence interval are shown.

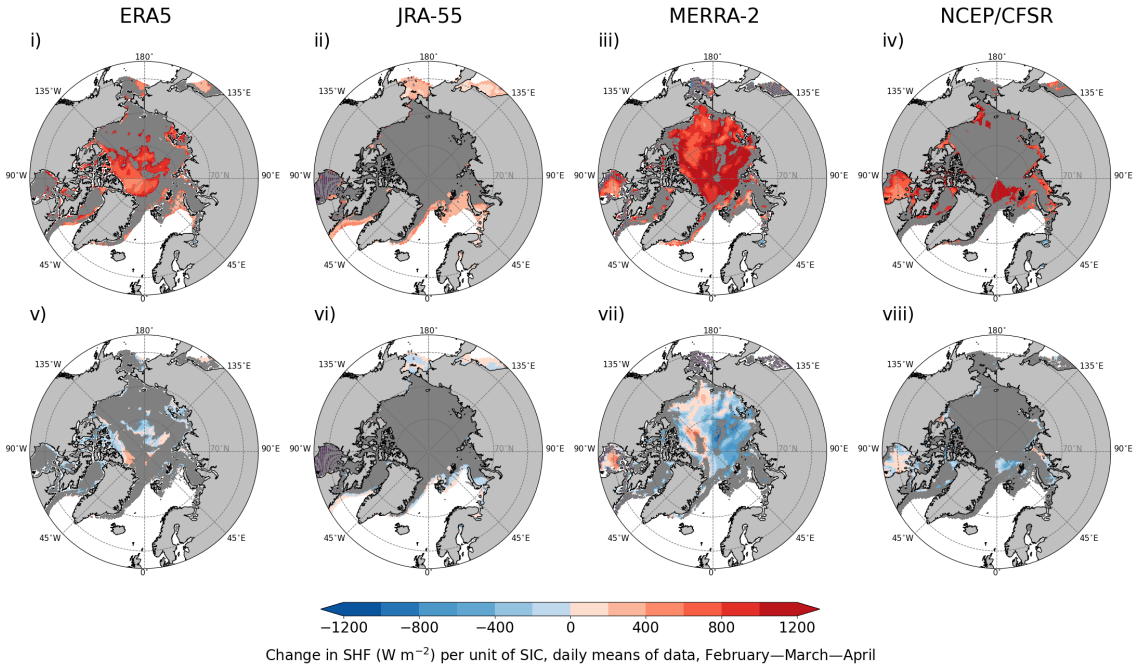

Figure S 6: Change in sensible heat flux (W m^{-2}) per unit of change in sea-ice concentration (slope of regression line) as represented in four reanalyses (columns), marine Arctic, FMA, based on the linear orthogonal-distance-regression (ODR) model. **i–iv** depict the period 1980–2000, **v–viii** show the 2001–2021 difference from 1980–2000. Dark grey indicates areas where the ODR model did not converge; in v–viii, dark grey shows these areas in 1980–2000 and/or 2001–2021. Only grid cells with a mean of SIC > 0.5 were considered, and only statistically significant results within 95 % confidence interval are shown.

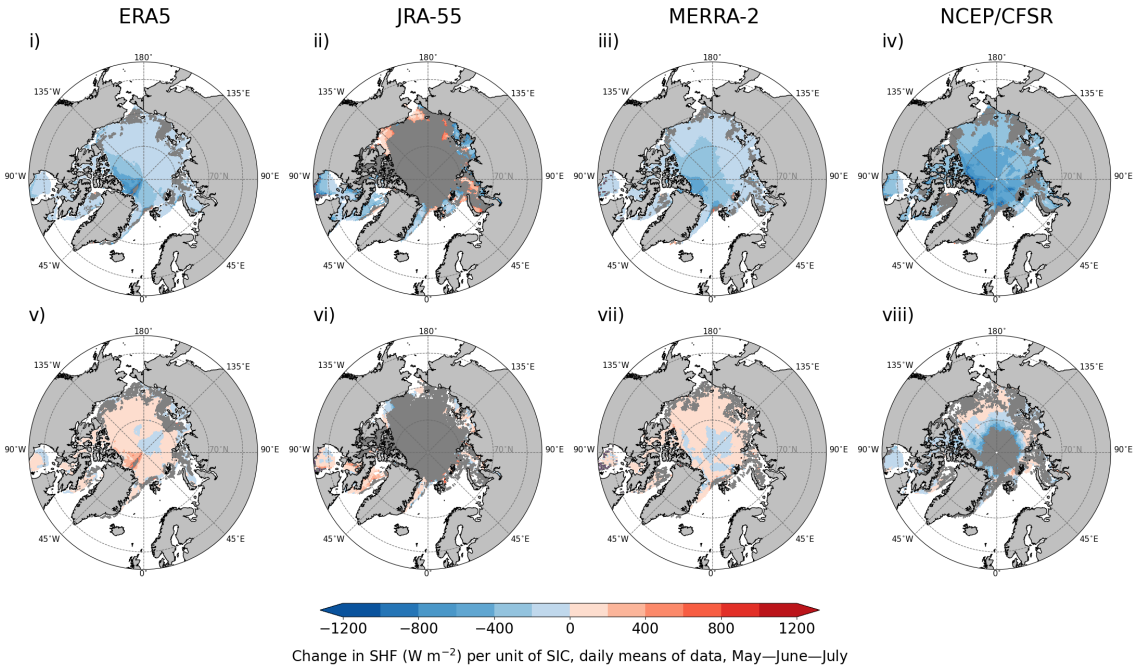

Figure S 7: Change in sensible heat flux (W m^{-2}) per unit of change in sea-ice concentration (slope of regression line) as represented in four reanalyses (columns), marine Arctic, MJJ, based on the linear orthogonal-distance-regression (ODR) model. **i–iv** depict the period 1980–2000, **v–viii** show the 2001–2021 difference from 1980–2000. Dark grey indicates areas where the ODR model did not converge; in v–viii, dark grey shows these areas in 1980–2000 and/or 2001–2021. Only grid cells with a mean of SIC > 0.5 were considered, and only statistically significant results within 95 % confidence interval are shown.

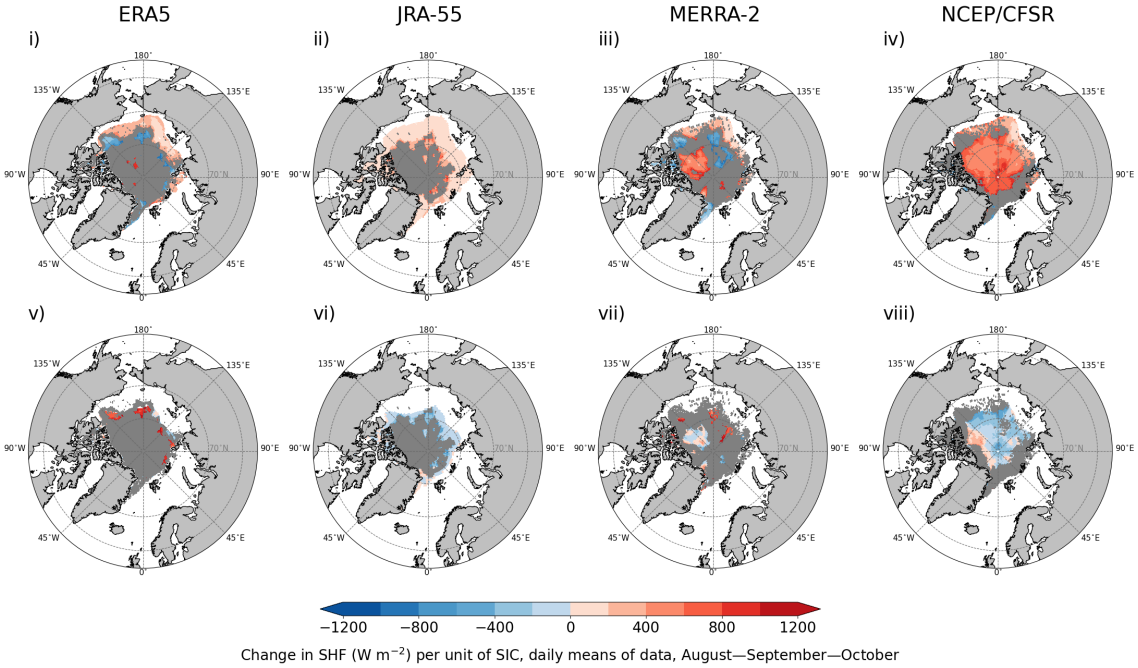

Figure S 8: Change in sensible heat flux (W m^{-2}) per unit of change in sea-ice concentration (slope of regression line) as represented in four reanalyses (columns), marine Arctic, ASO, based on the linear orthogonal-distance-regression (ODR) model. **i–iv** depict the period 1980–2000, **v–viii** show the 2001–2021 difference from 1980–2000. Dark grey indicates areas where the ODR model did not converge; in v–viii, dark grey shows these areas in 1980–2000 and/or 2001–2021. Only grid cells with a mean of SIC > 0.5 were considered, and only statistically significant results within 95 % confidence interval are shown.

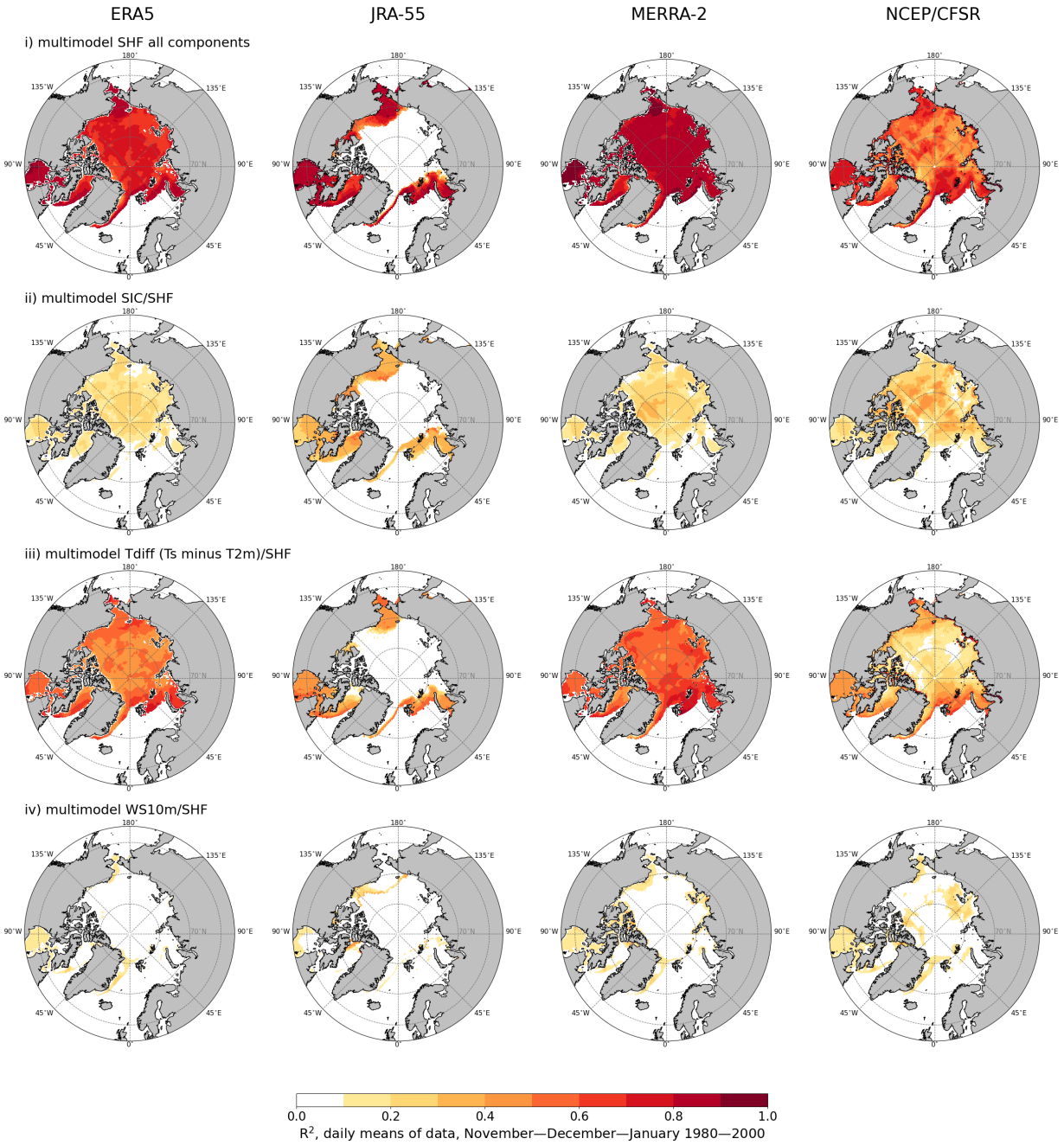

Figure S 9: Proportion of variance in the sensible heat flux (vSHF) explained by the linear ordinary-least-square regression model (coefficient of determination, R^2); daily means of data, NDJ, 1980–2000. Row **i** - vSHF explained by all components: SIC/temperature difference (T_s minus T_{2m}, T_{diff})/wind speed (10 m, WS_{10m}); row **ii** - vSHF explained by the SIC/SHF component of the model; row **iii** - vSHF explained by the T_{diff}/SHF component of the model; row **iv** - vSHF explained by the WS_{10m}/SHF component of the model. Only grid cells with a mean of SIC > 0.5 were considered.

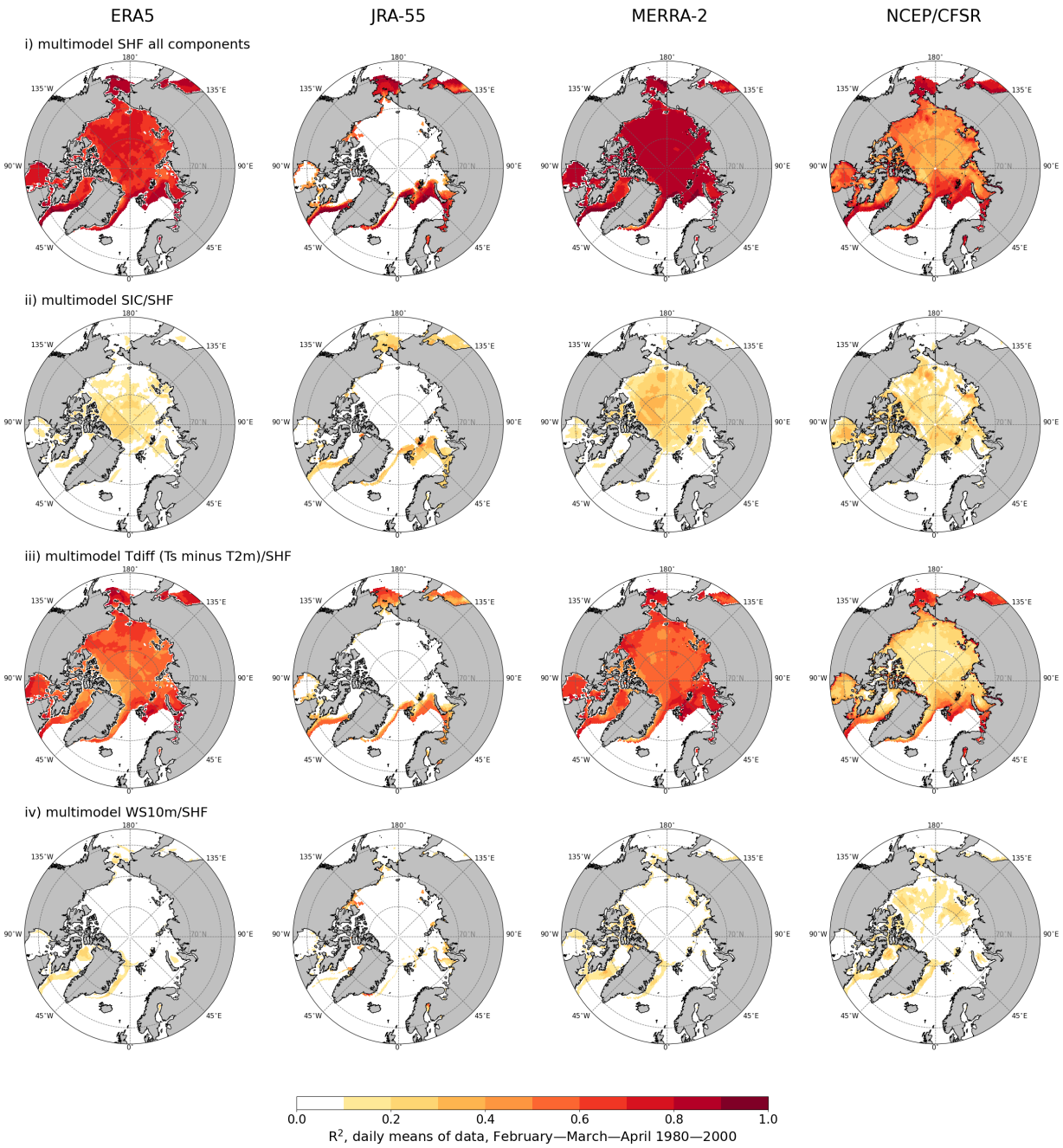

Figure S 10: Proportion of variance in the sensible heat flux (vSHF) explained by the linear ordinary-least-square regression model (coefficient of determination, R^2); daily means of data, FMA, 1980–2000. Row **i** - vSHF explained by all components: SIC/temperature difference (T_s minus T_{2m}, T_{diff})/wind speed (10 m, WS_{10m}); row **ii** - vSHF explained by the SIC/SHF component of the model; row **iii** - vSHF explained by the T_{diff}/SHF component of the model; row **iv** - vSHF explained by the WS_{10m}/SHF component of the model. Only grid cells with a mean of SIC > 0.5 were considered.

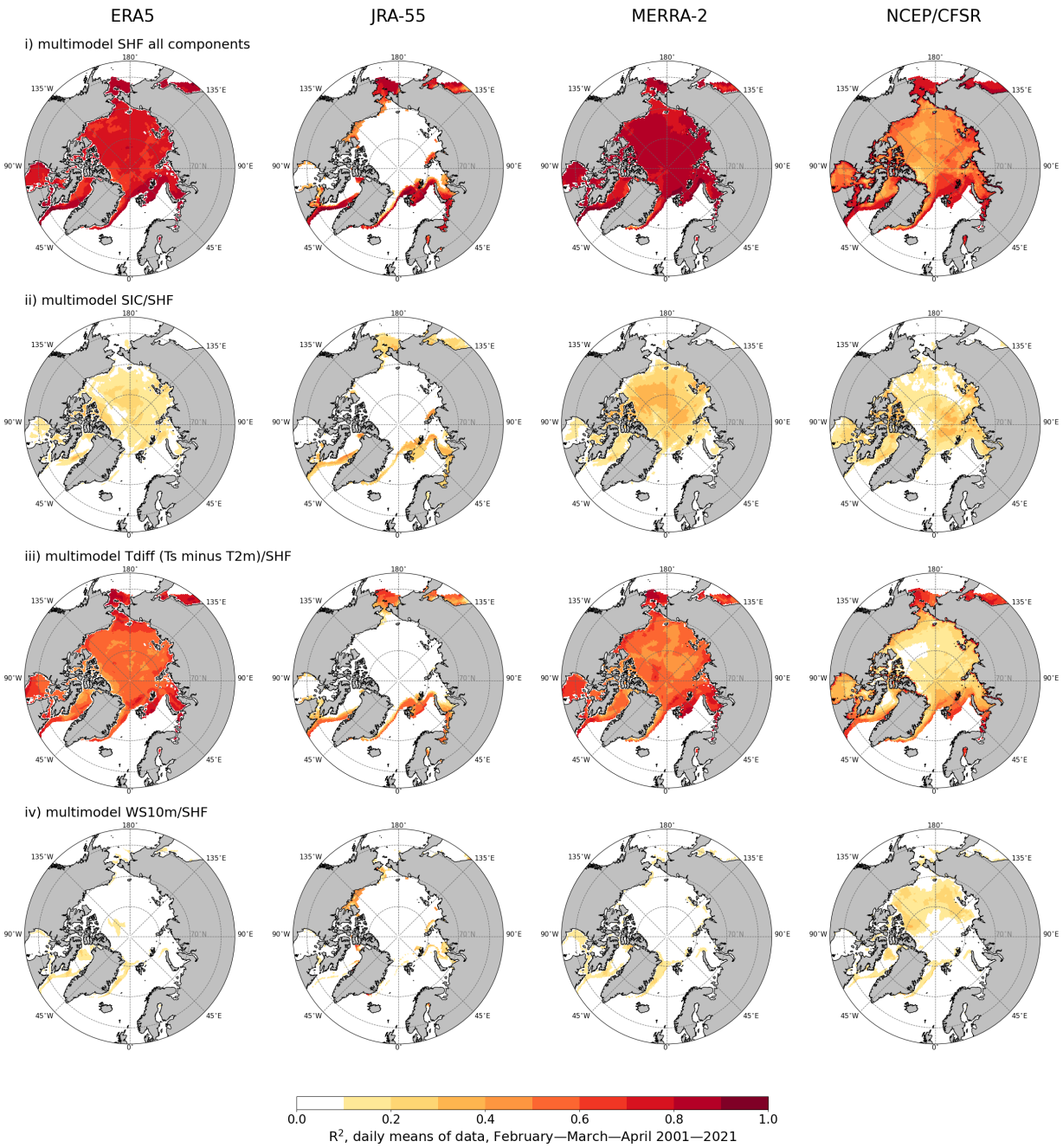

Figure S 11: Proportion of variance in the sensible heat flux (vSHF) explained by the linear ordinary-least-square regression model (coefficient of determination, R^2); daily means of data, FMA, 2001–2021. Row **i** - vSHF explained by all components: SIC/temperature difference (T_s minus T_{2m}, T_{diff})/wind speed (10 m, WS_{10m}); row **ii** - vSHF explained by the SIC/SHF component of the model; row **iii** - vSHF explained by the T_{diff}/SHF component of the model; row **iv** - vSHF explained by the WS_{10m}/SHF component of the model. Only grid cells with a mean of SIC > 0.5 were considered.

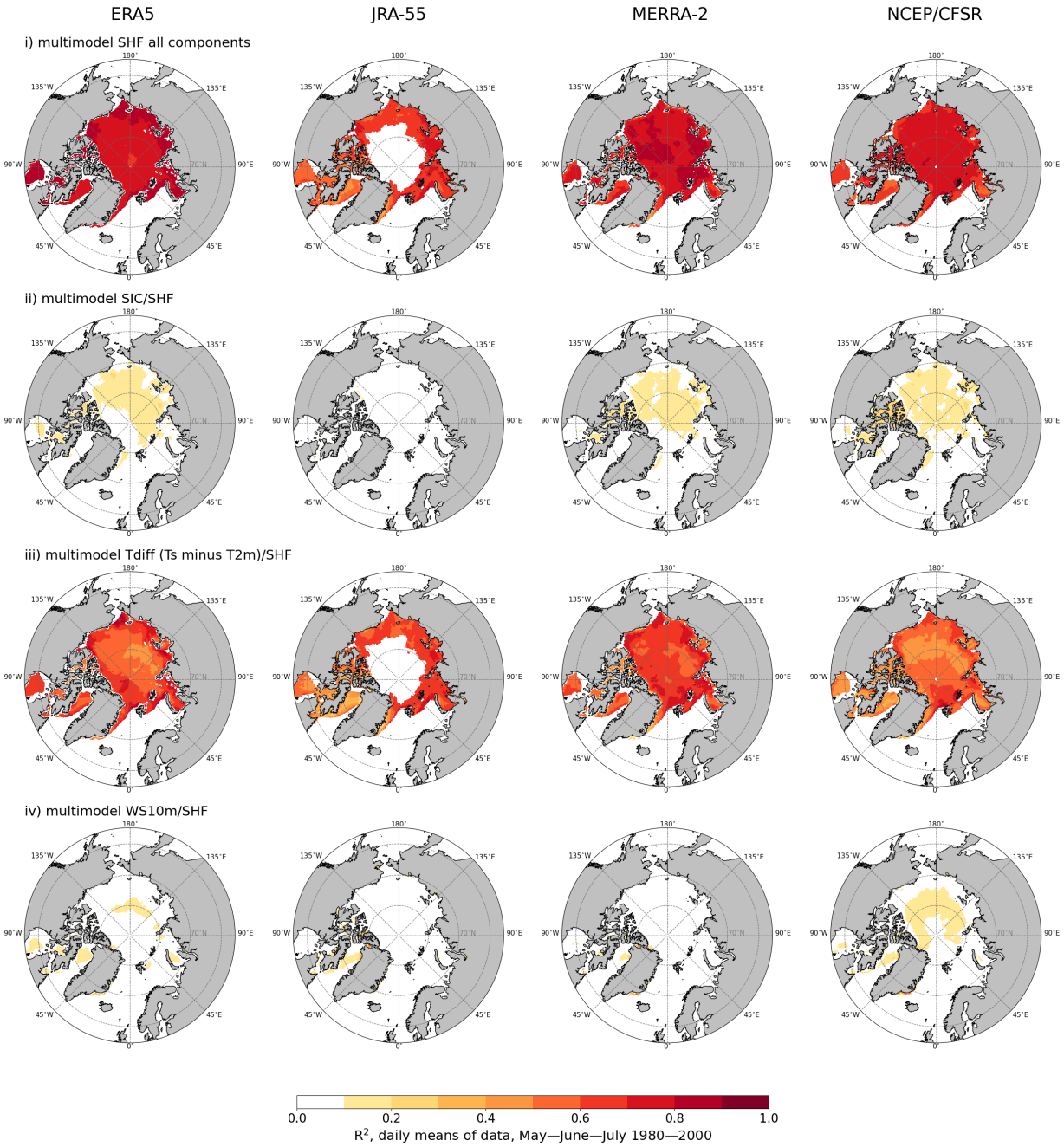

Figure S 12: Proportion of variance in the sensible heat flux (vSHF) explained by the linear ordinary-least-square regression model (coefficient of determination, R^2); daily means of data, MJJ, 1980–2000. Row **i** - vSHF explained by all components: SIC/temperature difference (T_s minus T_{2m}, T_{diff})/wind speed (10 m, WS_{10m}); row **ii** - vSHF explained by the SIC/SHF component of the model; row **iii** - vSHF explained by the T_{diff}/SHF component of the model; row **iv** - vSHF explained by the WS_{10m}/SHF component of the model. Only grid cells with a mean of SIC > 0.5 were considered.

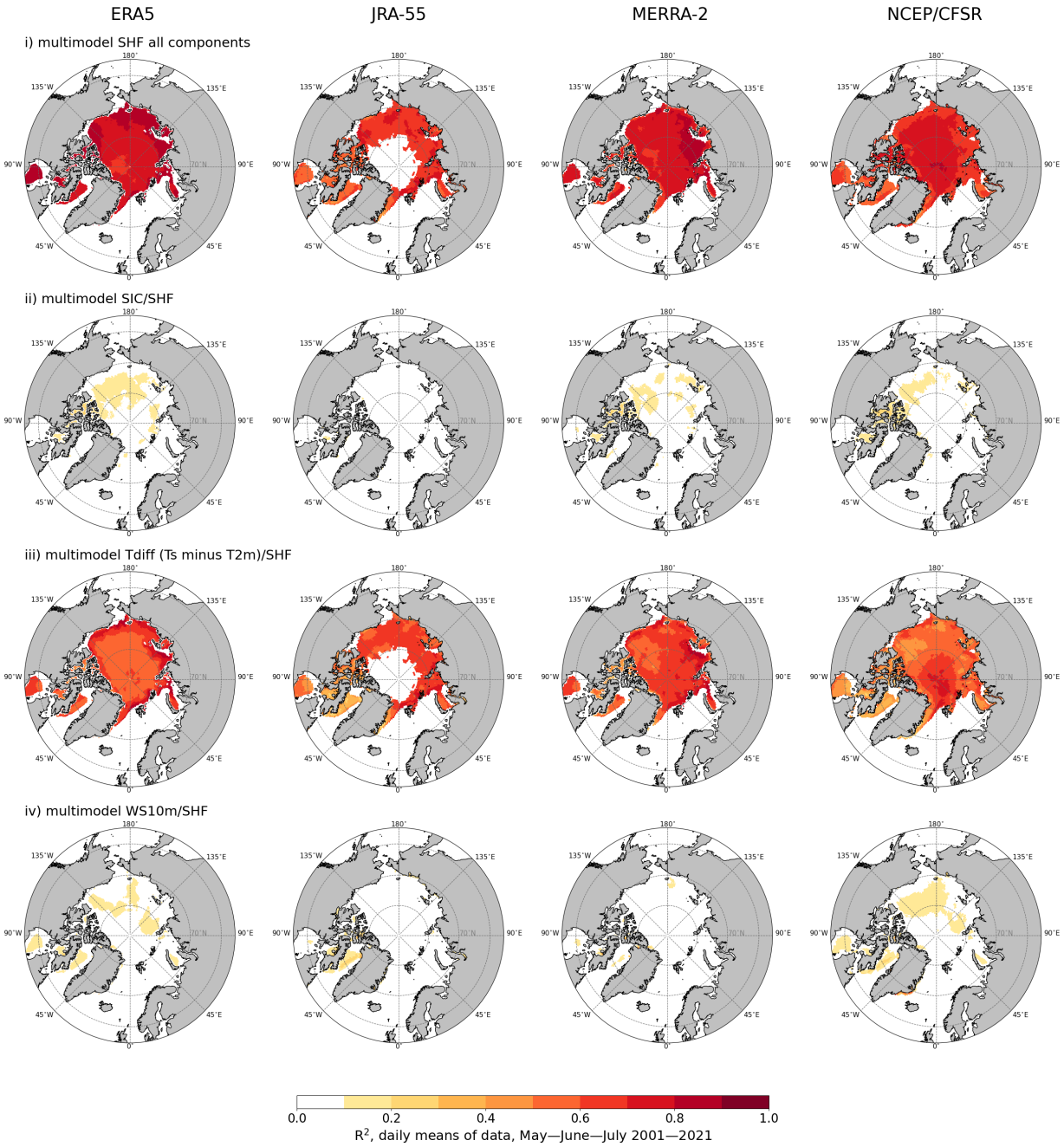

Figure S 13: Proportion of variance in the sensible heat flux (vSHF) explained by the linear ordinary-least-square regression model (coefficient of determination, R^2); daily means of data, MJJ, 2001–2021. Row **i** - vSHF explained by all components: SIC/temperature difference (T_s minus T_{2m}, T_{diff})/wind speed (10 m, WS_{10m}); row **ii** - vSHF explained by the SIC/SHF component of the model; row **iii** - vSHF explained by the T_{diff}/SHF component of the model; row **iv** - vSHF explained by the WS_{10m}/SHF component of the model. Only grid cells with a mean of SIC > 0.5 were considered.

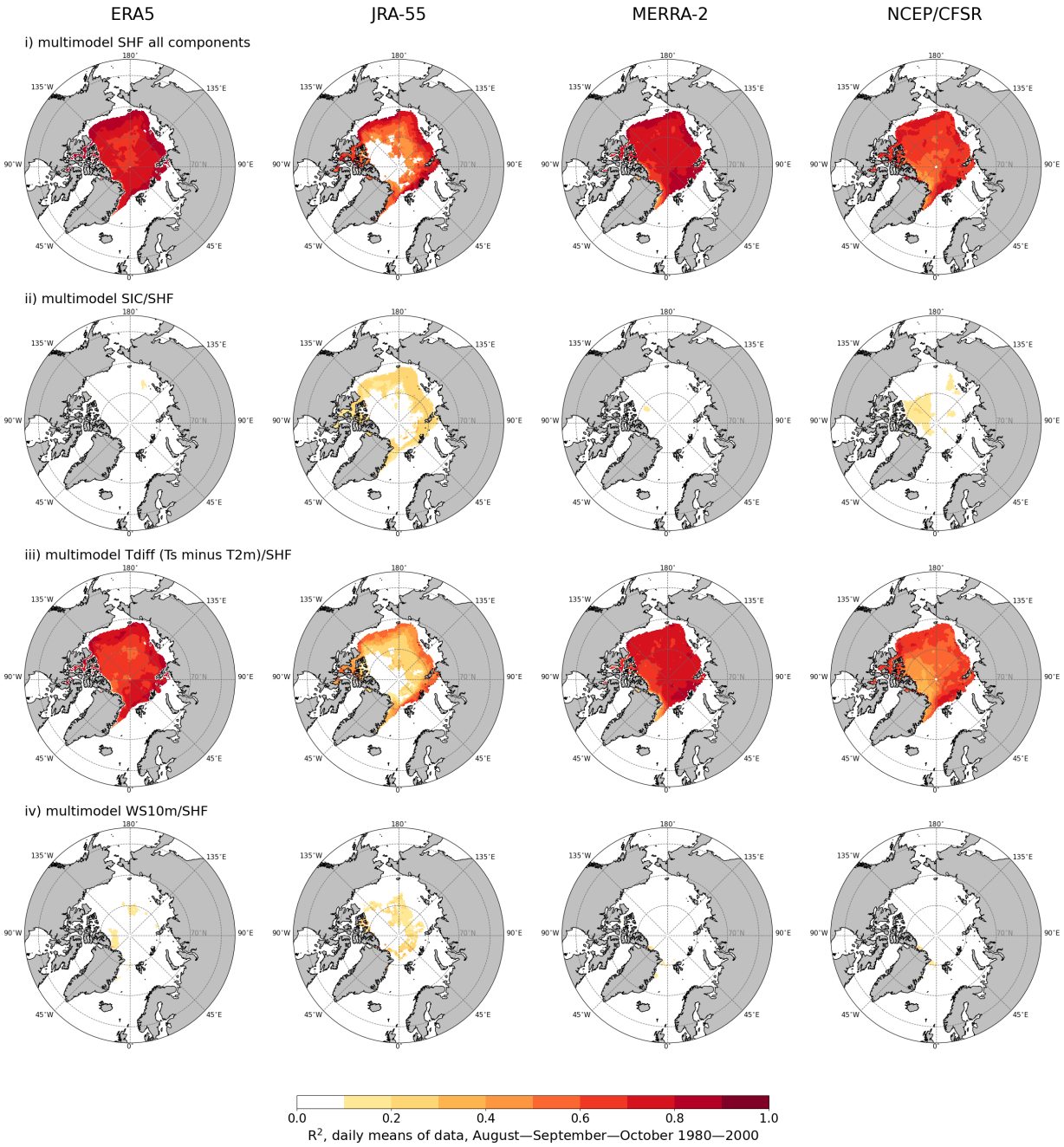

Figure S 14: Proportion of variance in the sensible heat flux (vSHF) explained by the linear ordinary-least-square regression model (coefficient of determination, R^2); daily means of data, ASO, 1980–2000. Row **i** - vSHF explained by all components: SIC/temperature difference (T_s minus T_{2m}, T_{diff})/wind speed (10 m, WS_{10m}); row **ii** - vSHF explained by the SIC/SHF component of the model; row **iii** - vSHF explained by the T_{diff}/SHF component of the model; row **iv** - vSHF explained by the WS_{10m}/SHF component of the model. Only grid cells with a mean of SIC > 0.5 were considered.

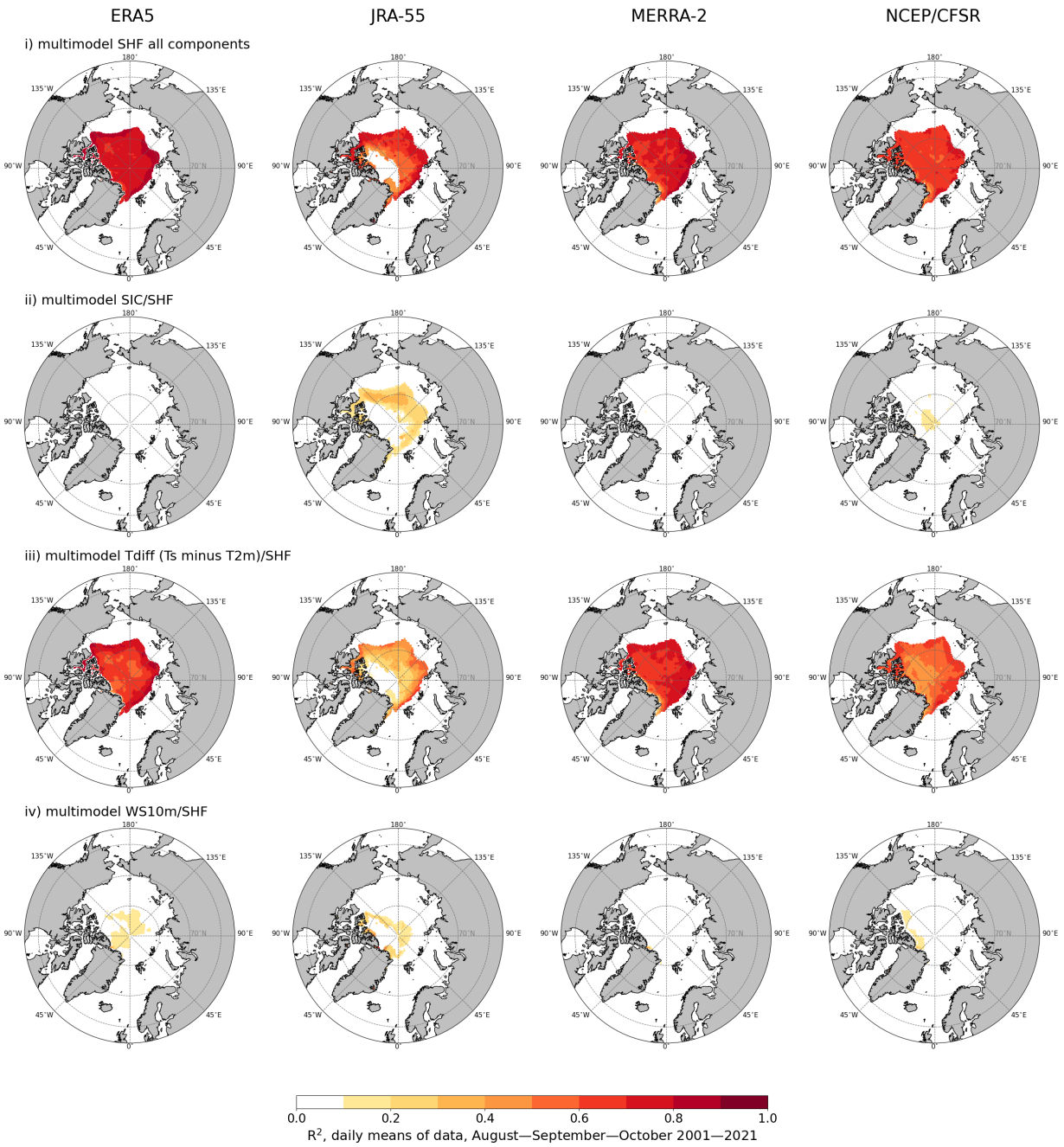

Figure S 15: Proportion of variance in the sensible heat flux (vSHF) explained by the linear ordinary-least-square regression model (coefficient of determination, R^2); daily means of data, ASO, 2001–2021. Row **i** - vSHF explained by all components: SIC/temperature difference (T_s minus T_{2m}, T_{diff})/wind speed (10 m, WS_{10m}); row **ii** - vSHF explained by the SIC/SHF component of the model; row **iii** - vSHF explained by the T_{diff}/SHF component of the model; row **iv** - vSHF explained by the WS_{10m}/SHF component of the model. Only grid cells with a mean of SIC > 0.5 were considered.

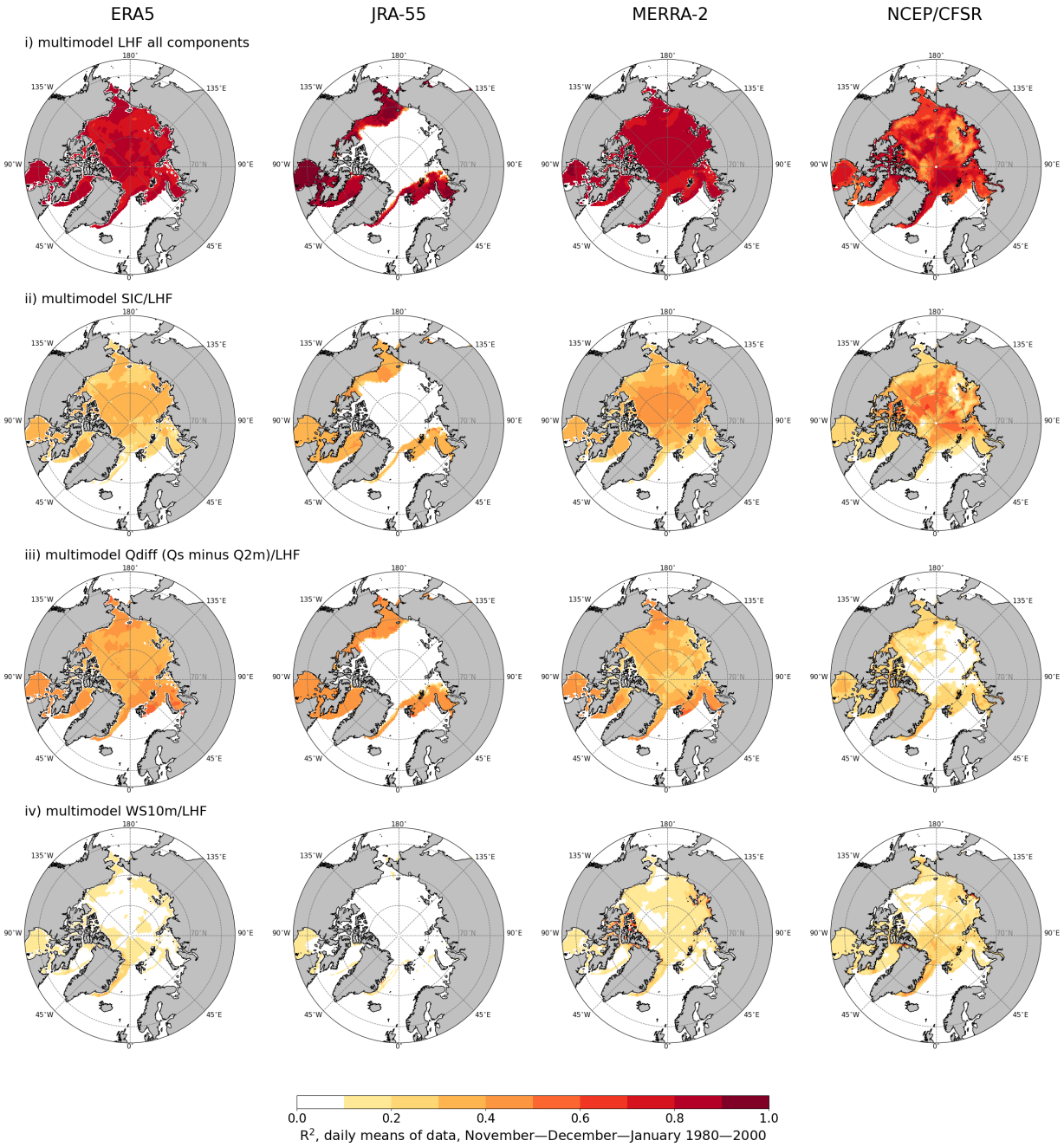

Figure S 16: Proportion of variance in the latent heat flux (vLHF) explained by the linear ordinary-least-square regression model (coefficient of determination, R^2); daily means of data, NDJ, 1980–2000. Row **i** - vLHF explained by all components: SIC/specific-humidity difference (Q_s minus Q_{2m}, Q_{diff})/wind speed (10 m, WS_{10m}); row **ii** - vLHF explained by the SIC/LHF component of the model; row **iii** - vLHF explained by the Q_{diff}/LHF component of the model; row **iv** - vLHF explained by the WS_{10m}/LHF component of the model. Only grid cells with a mean of SIC > 0.5 were considered.

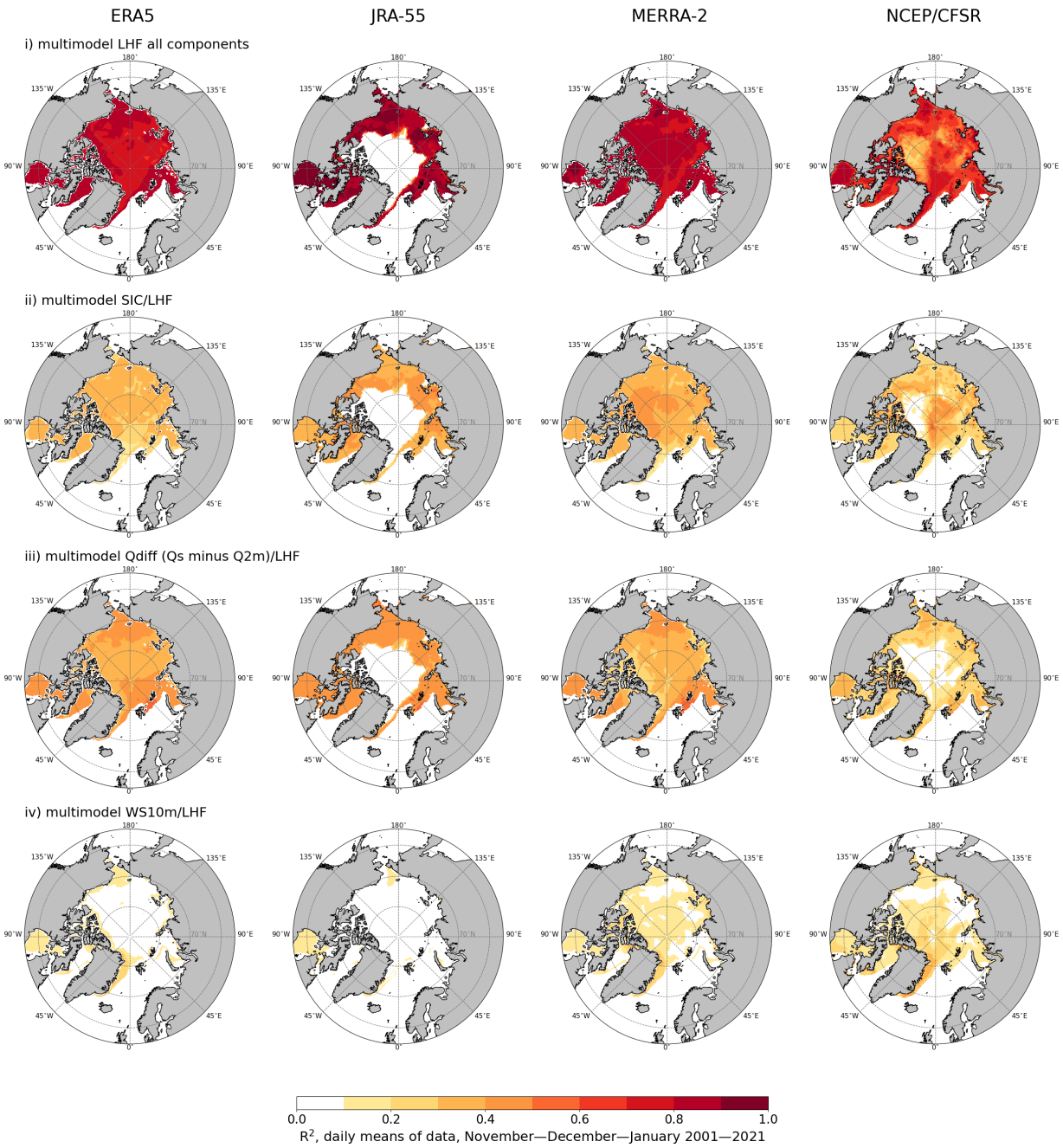

Figure S 17: Proportion of variance in the latent heat flux (vLHF) explained by the linear ordinary-least-square regression model (coefficient of determination, R^2); daily means of data, NDJ, 2001–2021. Row **i** - vLHF explained by all components: SIC/specific-humidity difference (Q_s minus Q_{2m}, Q_{diff})/wind speed (10 m, WS_{10m}); row **ii** - vLHF explained by the SIC/LHF component of the model; row **iii** - vLHF explained by the Q_{diff}/LHF component of the model; row **iv** - vLHF explained by the WS_{10m}/LHF component of the model. Only grid cells with a mean of SIC > 0.5 were considered.

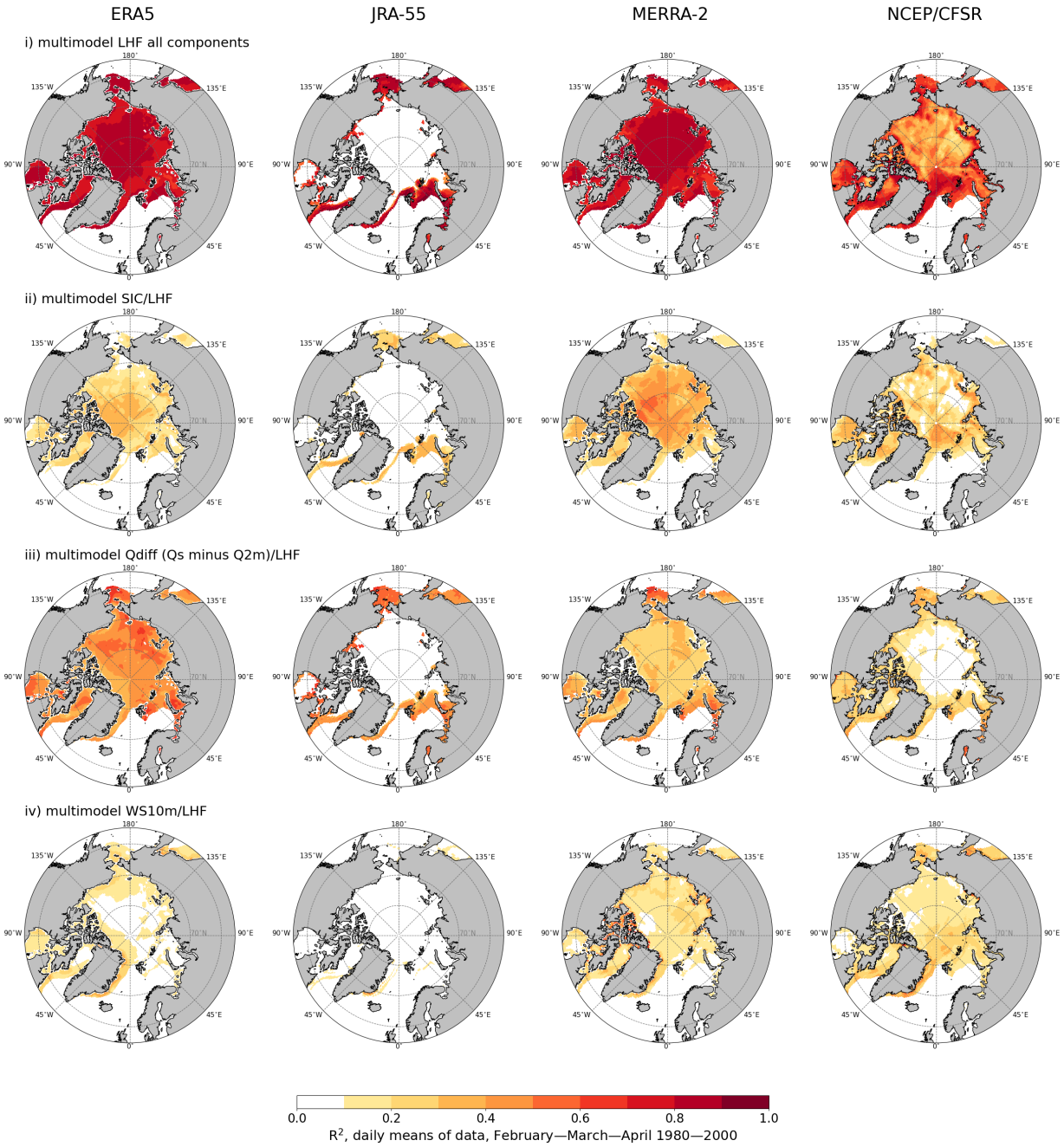

Figure S 18: Proportion of variance in the latent heat flux (vLHF) explained by the linear ordinary-least-square regression model (coefficient of determination, R^2); daily means of data, FMA, 1980–2000. Row **i** - vLHF explained by all components: SIC/specific-humidity difference (Q_s minus Q_{2m}, Q_{diff})/wind speed (10 m, WS_{10m}); row **ii** - vLHF explained by the SIC/LHF component of the model; row **iii** - vLHF explained by the Q_{diff}/LHF component of the model; row **iv** - vLHF explained by the WS_{10m}/LHF component of the model. Only grid cells with a mean of SIC > 0.5 were considered.

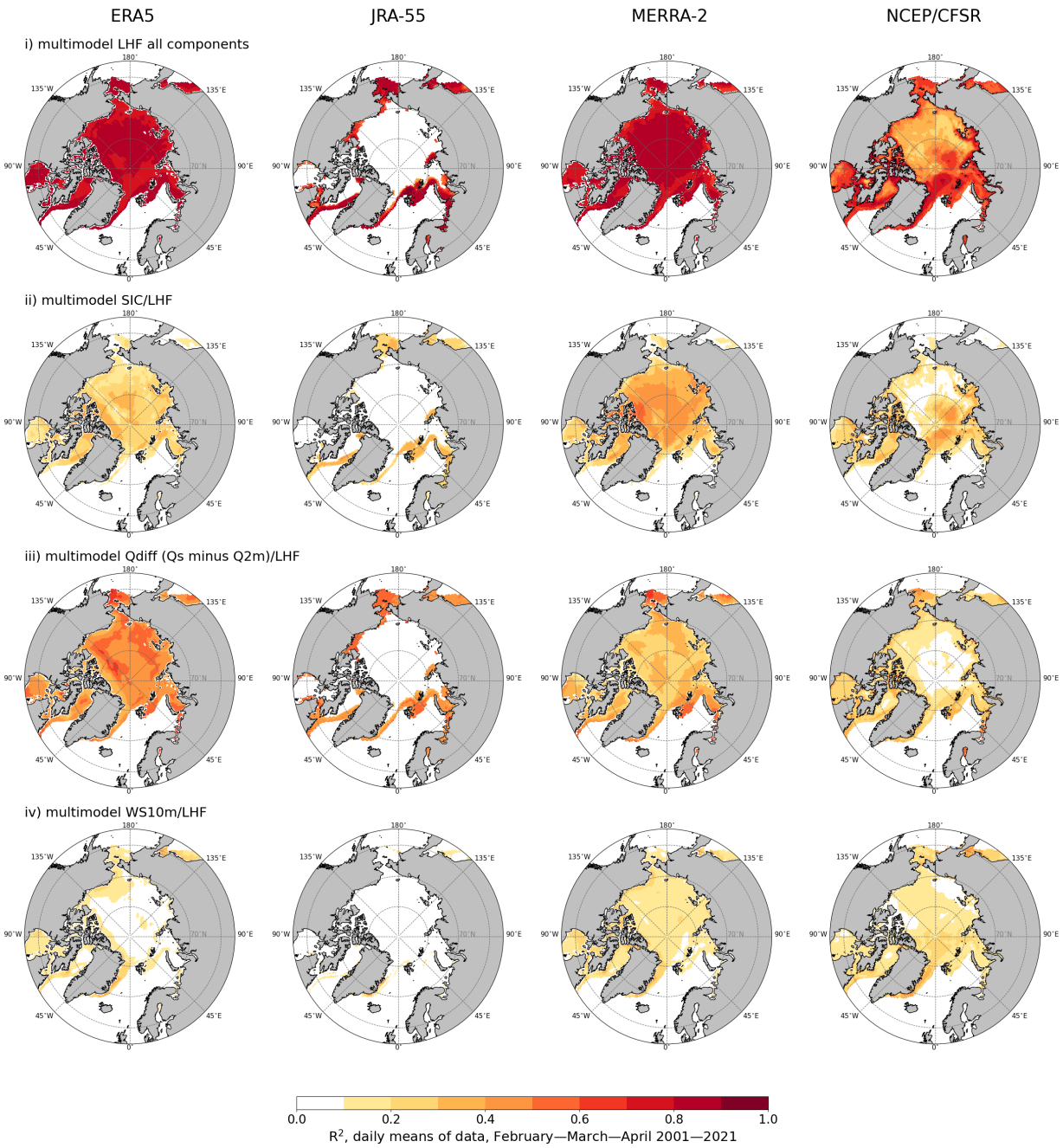

Figure S 19: Proportion of variance in the latent heat flux (vLHF) explained by the linear ordinary-least-square regression model (coefficient of determination, R^2); daily means of data, FMA, 2001–2021. Row **i** - vLHF explained by all components: SIC/specific-humidity difference (Q_s minus Q_{2m}, Q_{diff})/wind speed (10 m, WS_{10m}); row **ii** - vLHF explained by the SIC/LHF component of the model; row **iii** - vLHF explained by the Q_{diff}/LHF component of the model; row **iv** - vLHF explained by the WS_{10m}/LHF component of the model. Only grid cells with a mean of SIC > 0.5 were considered.

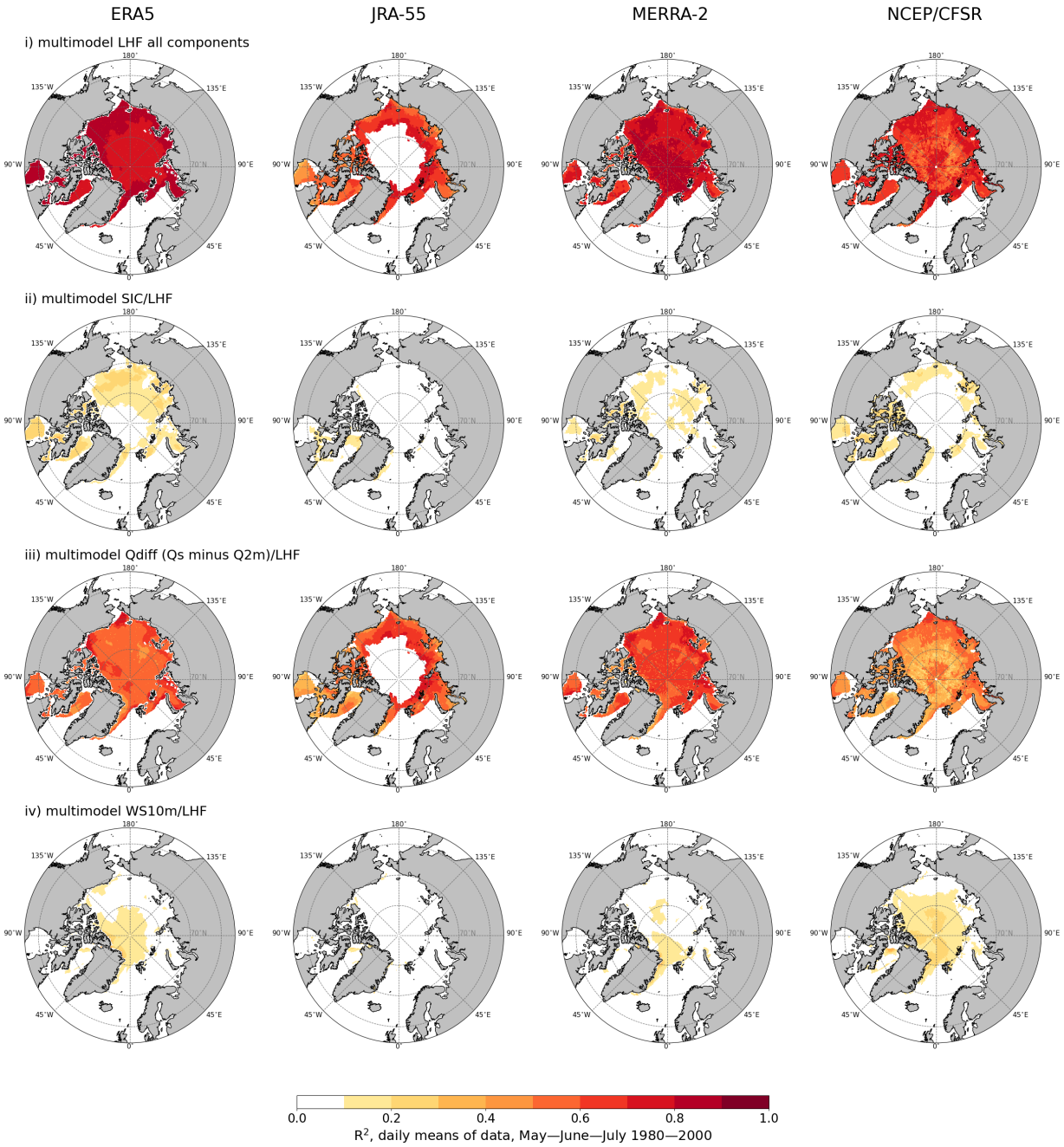

Figure S 20: Proportion of variance in the latent heat flux (vLHF) explained by the linear ordinary-least-square regression model (coefficient of determination, R^2); daily means of data, MJJ, 1980–2000. Row **i** - vLHF explained by all components: SIC/specific-humidity difference (Q_s minus Q_{2m}, Q_{diff})/wind speed (10 m, WS_{10m}); row **ii** - vLHF explained by the SIC/LHF component of the model; row **iii** - vLHF explained by the Q_{diff}/LHF component of the model; row **iv** - vLHF explained by the WS_{10m}/LHF component of the model. Only grid cells with a mean of SIC > 0.5 were considered.

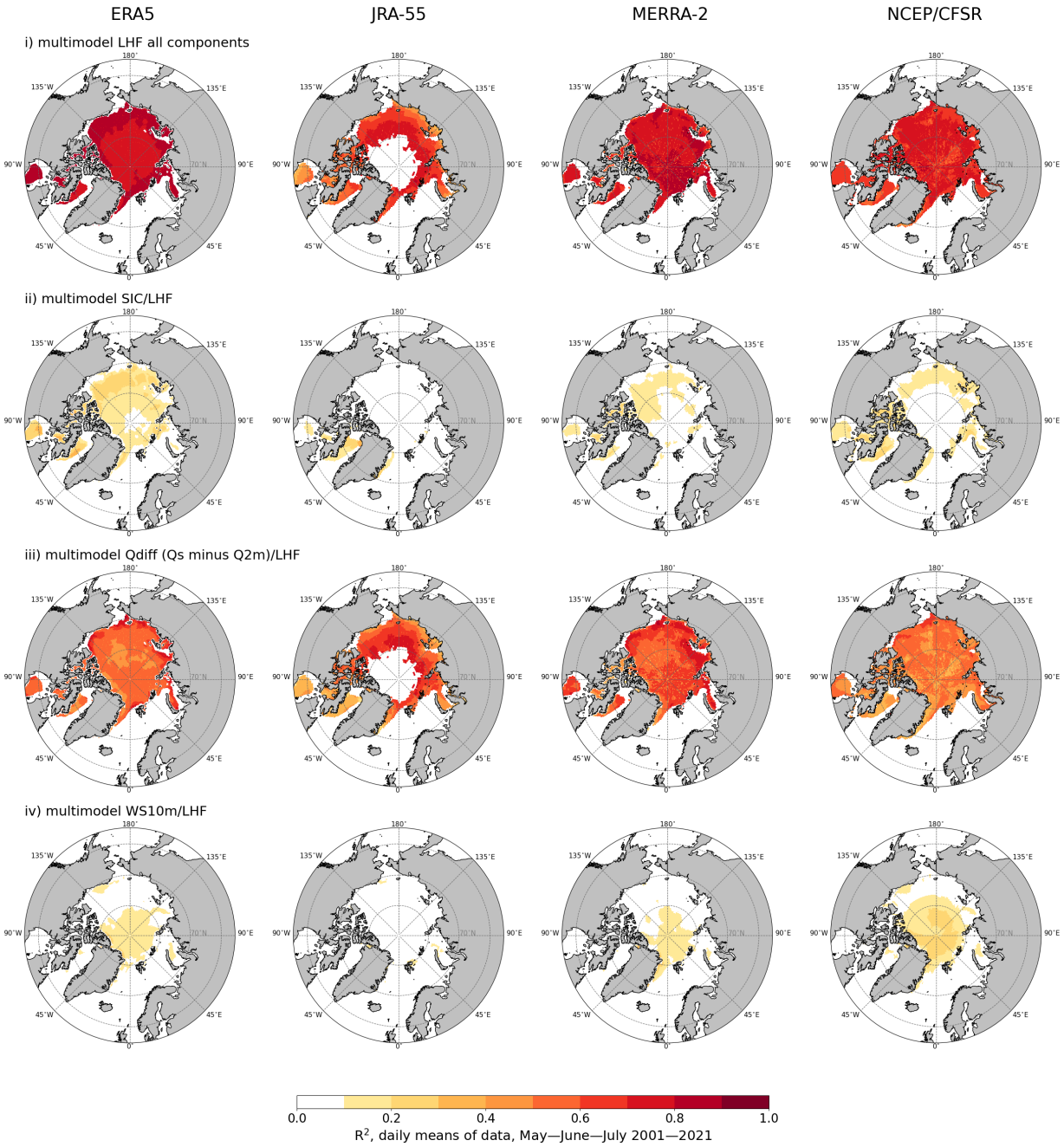

Figure S 21: Proportion of variance in the latent heat flux (vLHF) explained by the linear ordinary-least-square regression model (coefficient of determination, R^2); daily means of data, MJJ, 2001–2021. Row **i** - vLHF explained by all components: SIC/specific-humidity difference (Q_s minus Q_{2m}, Q_{diff})/wind speed (10 m, WS_{10m}); row **ii** - vLHF explained by the SIC/LHF component of the model; row **iii** - vLHF explained by the Q_{diff}/LHF component of the model; row **iv** - vLHF explained by the WS_{10m}/LHF component of the model. Only grid cells with a mean of SIC > 0.5 were considered.

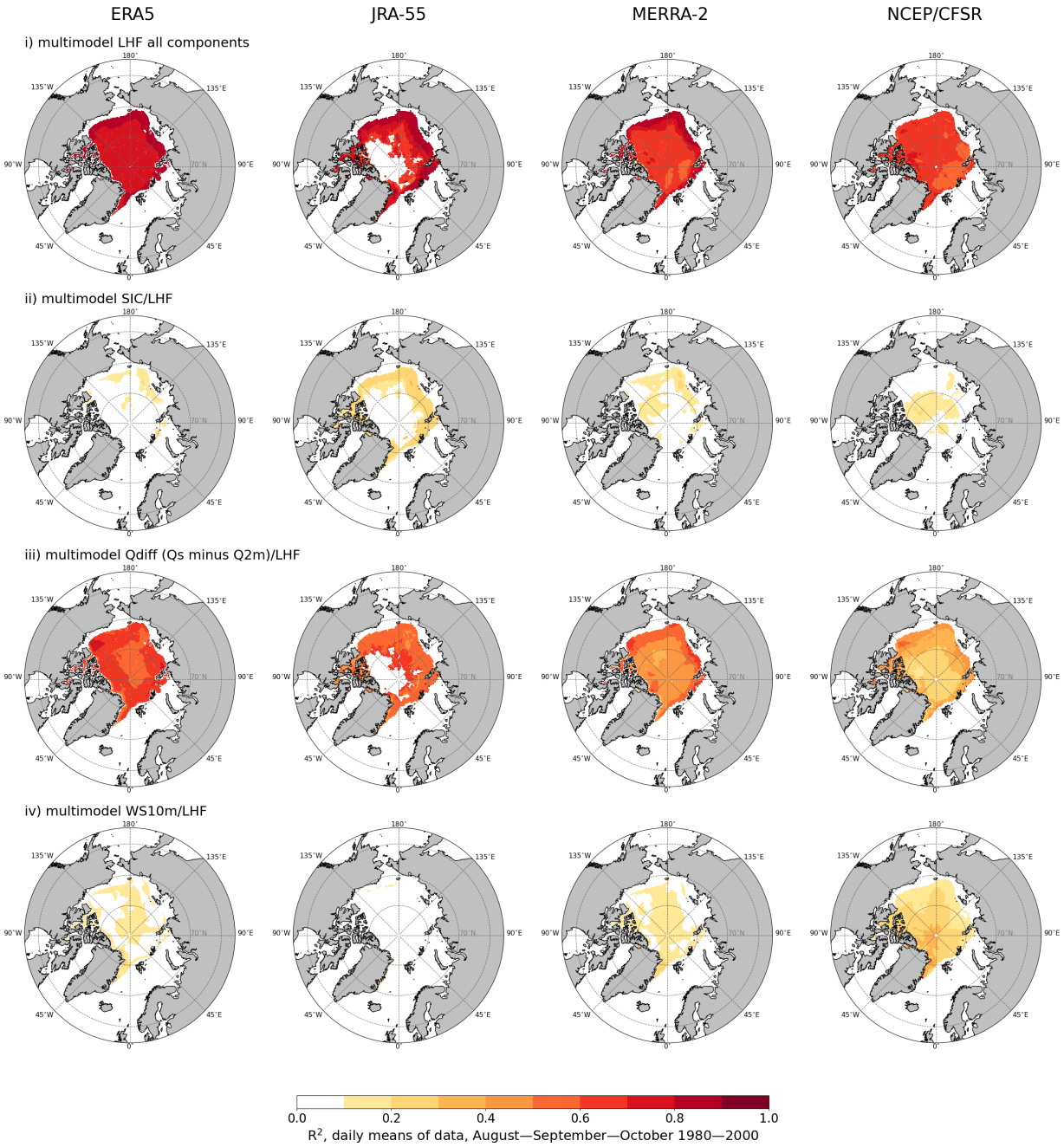

Figure S 22: Proportion of variance in the latent heat flux (vLHF) explained by the linear ordinary-least-square regression model (coefficient of determination, R^2); daily means of data, ASO, 1980–2000. Row **i** - vLHF explained by all components: SIC/specific-humidity difference (Q_s minus Q_{2m}, Q_{diff})/wind speed (10 m, WS_{10m}); row **ii** - vLHF explained by the SIC/LHF component of the model; row **iii** - vLHF explained by the Q_{diff}/LHF component of the model; row **iv** - vLHF explained by the WS_{10m}/LHF component of the model. Only grid cells with a mean of SIC > 0.5 were considered.

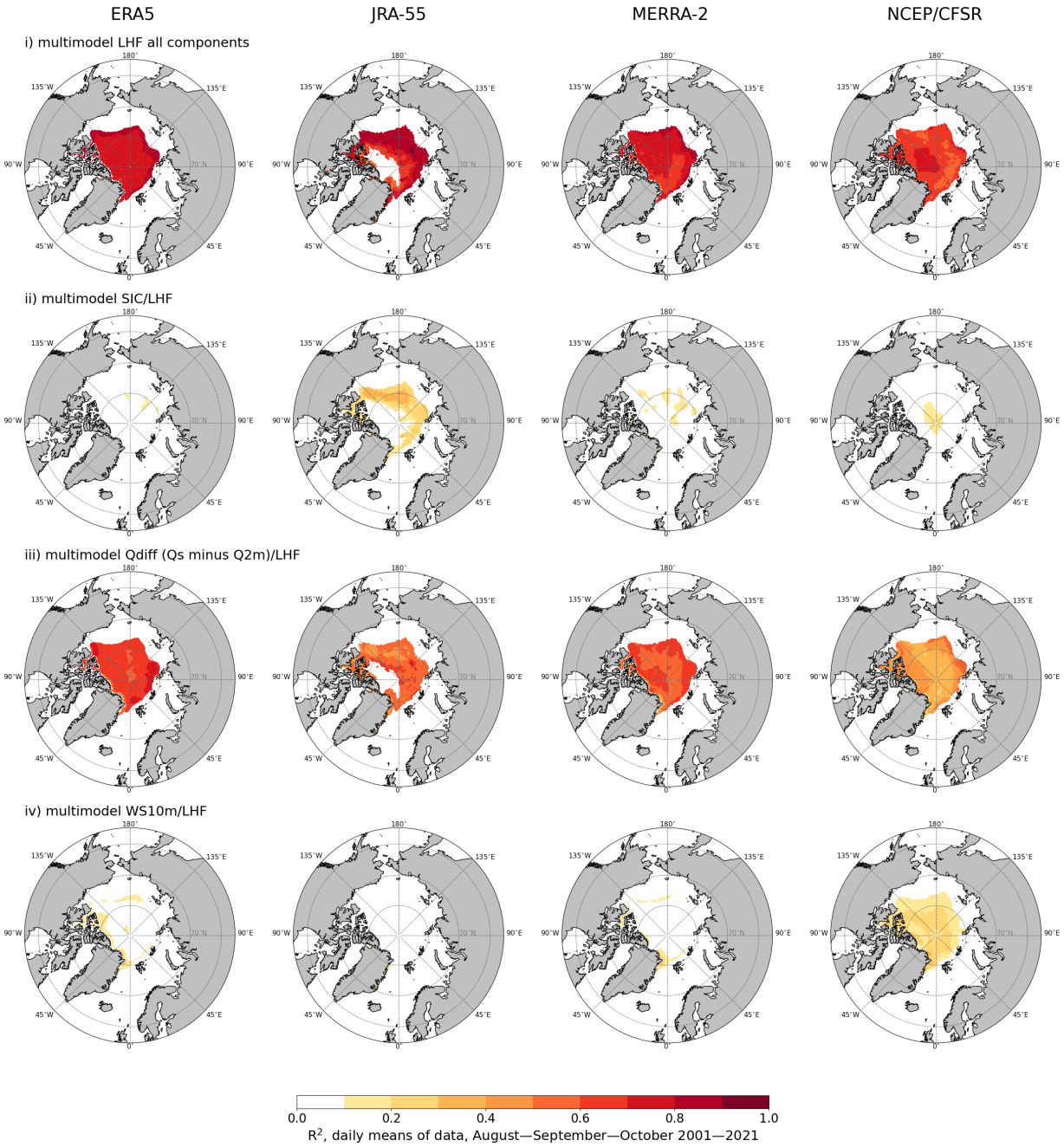

Figure S 23: Proportion of variance in the latent heat flux (vLHF) explained by the linear ordinary-least-square regression model (coefficient of determination, R^2); daily means of data, ASO, 2001–2021. Row **i** - vLHF explained by all components: SIC/specific-humidity difference (Q_s minus Q_{2m}, Q_{diff})/wind speed (10 m, WS_{10m}); row **ii** - vLHF explained by the SIC/LHF component of the model; row **iii** - vLHF explained by the Q_{diff}/LHF component of the model; row **iv** - vLHF explained by the WS_{10m}/LHF component of the model. Only grid cells with a mean of SIC > 0.5 were considered.